GRADO DE FÍSICA

UNIVERSIDAD DE LA LAGUNA

TRABAJO FIN DE GRADO

Aplicaciones ópticas de microesferas transparentes

Autor: Daniel Walo Martín

Tutores: Inocencio Rafael Martín Benenzuela

Susana Ríos Rodríguez

Index

Abstract.....3

Objetivos del trabajo.....4

Introducción.....5

Theoretical background.....7

Rare earth ions.....7

Electronic structure and energy levels. Cerium and Neodymium.....7

Photon upconversion 9

Energy Transfer processes.....11

Fluorescence Intensity Ratio (FIR) 12

Whispering Gallery Modes (WGM) 13

Thermal Sensors 14

Experimental Methods 16

Microsphere production.....16

Temperature Calibration.....16

Optical Measurements.....17

Results and discussion.....20

Temperature Calibration.....20

Displacement of the WGM 21

Laser emission 25

Upconversion 26

Time resolved experiments 28

Conclusions.....30

References.....32

Abstract

Los materiales ópticos dopados con iones lantánidos como el Nd^{3+} presentan una serie de propiedades ópticas que los hacen útiles para el desarrollo de sensores ópticos de temperatura. Algunos de estos iones presentan niveles de energía cuya proximidad favorece que se produzca una distribución de población entre ellos que cambia con la temperatura. En consecuencia, se puede determinar la temperatura del material huésped que los contiene si se conoce previamente como cambia la población de estos niveles con la temperatura.

Si se construyen microesferas con materiales dopados con estos iones, es posible sacar provecho de otras propiedades relacionadas con las características ópticas de las mismas. Las microesferas son cavidades resonantes hechas de materiales dieléctricos transparentes que amplifican ciertas longitudes de onda en su interior llamadas modos resonantes. Por lo tanto, si se excita una microesfera dopada, la emisión de los iones en su interior experimenta una serie de reflexiones en su interior que hace que se amplifiquen algunas longitudes de onda. Esto produce que en el espectro de emisión de los iones aparezcan picos estrechos en las posiciones de las longitudes de onda resonantes. Los cambios en la temperatura de la microesfera producen variaciones en sus dimensiones y en su índice de refracción lo que provoca que varíe la longitud de onda de los modos.

En este trabajo se han utilizado microesferas de vidrio dopadas con iones de Ce^{3+} y de Nd^{3+} y se ha estudiado como cambia la longitud de onda de los modos resonantes en función de la temperatura de la microesfera. Esto ha sido posible gracias a una calibración previa de la emisión de la muestra de vidrio para distintas temperaturas.

Si se desea optimizar la intensidad de la emisión, se deben estudiar los procesos de transferencia de energía no radiativa entre los iones de la muestra para distintas concentraciones. Del análisis de las curvas de decaimiento de la intensidad con el tiempo y de los espectros de emisión es posible obtener la concentración del ion dopante óptima para obtener la máxima intensidad posible.

Si el material dopante puede producir emisión láser, es posible observar este tipo de emisión en la microesfera debido al gran número de reflexiones en su interior. Para ello se requieren muestras de gran esfericidad, así como excitar con distintas longitudes de onda para estudiar cuál es la más eficiente. Este tipo de emisión se ha observado a lo largo de este trabajo excitando de forma continua.

Objetivos del trabajo

El objetivo de este trabajo es analizar las propiedades ópticas de microesferas dopadas con iones trivalentes lantánidos. Los objetivos específicos se pueden resumir en los siguientes puntos:

- Analizar el efecto de termalización en el espectro de emisión de iones de neodimio usando la técnica “Fluorescence Intensity Ratio, (FIR)”.
- Observar los modos resonantes de una microesfera dopada con iones de cerio y neodimio.
- Analizar la dependencia con la temperatura de la longitud de onda de los modos resonantes de la microesfera.
- Comparar la dependencia con la temperatura de la longitud de onda de los modos resonantes de la microesfera con el efecto de termalización en la emisión de los iones de neodimio para concluir cuál de estas técnicas es más sensible a cambios de temperatura.
- Observar y analizar emisión láser en microrresonadores esféricos hechos de vidrio dopado con iones de cerio y neodimio.
- Observar el proceso de upconversion en microesferas.
- Analizar el mecanismo de upconversion en los iones de neodimio.
- Determinar si se están produciendo procesos de transferencia de energía entre los iones dopantes.

Introducción

Los iones ópticamente activos presentan propiedades luminiscentes que proporcionan información de las características del material en el que se encuentran. Los elementos químicos con emisiones fluorescentes, los quantum dots o las proteínas fluorescentes son usados comúnmente para estudiar el material huésped [1, 2]. Entre ellos, los iones trivalentes lantánidos son usados ampliamente porque presentan muchas transiciones fluorescentes en todo el rango óptico (desde el ultravioleta hasta el infrarrojo cercano) y pueden ser usados en distintos de materiales como pueden ser vidrios, cristales o el medio intracelular [3, 4].

En los últimos años, los avances en nanotecnología han fomentado el desarrollo de nuevos métodos para medir la temperatura [5]. Este es un parámetro importante porque la temperatura modifica la dinámica y funcionamiento de sistemas a micro y nano escala. Por ejemplo, en sistemas biológicos, la temperatura determina la velocidad a la que se producen procesos como la división celular [6].

Los sensores de temperatura convencionales (termistores y termopares) no se pueden utilizar para medir la temperatura de estos sistemas porque requieren contacto directo con ellos. En consecuencia, se ha desarrollado una nueva generación de sensores que aprovechan las propiedades ópticas de los materiales, los sensores ópticos. Estos dispositivos miden diferencias en las características de la emisión de los materiales (intensidad, longitud de onda de la emisión, tiempo de vida, forma de la banda) debidas a cambios en la temperatura [5] incluso a través del vacío [7]. Por otro lado, presentan el inconveniente de que precisan de análisis espectral y de medidas de alta precisión.

Algunos iones lantánidos triplemente ionizados presentan cambios en sus bandas de emisión debido a efectos de termalización [8-9]. En otras palabras, diferencias en temperatura causan variaciones en la intensidad de las bandas de emisión. Estas diferencias se deben a redistribuciones térmicas de población entre dos niveles energéticamente próximos que están acoplados a un mismo nivel de menor energía [10]. Este efecto se estudia a través de la técnica de "Fluorescence Intensity Ratio, (FIR)" que compara las intensidades fluorescentes de un material a distintas temperaturas. Es por ello que se han desarrollado varios sensores ópticos de temperatura basados en esta técnica usando iones lantánidos que presentan niveles de energía próximos entre sí [10-14].

Por otro lado, es posible medir la temperatura de un sistema usando microrresonadores esféricos. Entre ellos, las microesferas transparentes hechas de compuestos de sílica son las de uso más extendido. Si su índice de refracción es mayor que el del medio en el que se encuentran, la luz experimenta una sucesión de reflexiones internas totales en las paredes de la microesfera. Algunas de estas reflexiones vuelven a su punto de origen en fase, lo que produce un efecto de resonancia, dando lugar a los modos resonantes de la cavidad ("Whispering Gallery Modes,

WGM"). Una cavidad ideal sin pérdidas confinaría la luz en su interior indefinidamente. Las desviaciones de este sistema ideal se describen a través del factor de calidad, Q (que es proporcional al tiempo de confinamiento de la luz en el interior de la microesfera) [14]. Las microesferas presentan altos factores de calidad, lo que conduce a altas densidades de energía en su interior [15].

Otra consecuencia del alto factor de calidad de las microesferas es que producen picos muy estrechos en las longitudes de onda resonantes. Además, pequeños cambios en los parámetros de la microesfera (radio e índice de refracción) produce un desplazamiento en la longitud de onda del modo resonante. Si estas variaciones son consecuencia de cambios en la temperatura, esto puede aprovecharse para estimar la temperatura. Si la microesfera se dopa con iones ópticamente activos, estos picos aparecen superpuestos a la emisión de los iones.

Una aplicación más, es el desarrollo de dispositivos láser de baja potencia umbral. Si la microesfera es dopada con un material ópticamente activo que pueda producir emisión láser, esta actúa como una cavidad resonante y la emisión laser se obtiene cuando se alcanza la inversión de población. En lugar de introducir el material dopante en la microesfera, también es posible obtener emisión láser recubriendo una microesfera sin dopar con una capa del material activo [16].

Theoretical Background

This work is focused on the study of the emission spectra obtained with glass microspheres doped with optically active rare earth ions. Therefore, in this section we will introduce concepts that will be referred throughout the text. The first subsection comprises a general introduction to properties of optically active rare earth ions, including some specific characteristic of Ce^{3+} and Nd^{3+} ions. The second section introduces the Inokuti-Hirayama model to study the non radiative energy processes and the third one describes the physical mechanisms behind the FIR technique. Then the fourth subsection shows two different approaches to study the WGM resonances. Finally, the last section presents the parameters employed to characterise thermal sensors.

Rare Earth ions

Electronic structure and energy levels. Cerium and Neodymium

Lanthanide rare earth elements (elements with Z number from 57 to 71) present a great number of fluorescent transitions in the visible and near infrared spectrum. Its ground state electronic structure consists on a series of complete filled shells with the same structure as xenon, and a partially filled inner 4f shell. This orbital is very localised since it is shielded by the outer 5s and 5p shells. Rare earth ions are normally trivalent and the ionisation usually results in the removal of two 6s and one 4f electrons. Thus, the fluorescent emissions are given by 4f→4f optical transitions that remain almost unaffected by the host material where they are located, i.e. the ion-lattice interaction does not modify the overall pattern of the spectrum. The electronic configuration of neodymium and cerium ions in its trivalent form are [17]:

$$Ce^{3+}: \ldots 4f^{1}5s^{2}5p^{6}$$

$$Nd^{3+}: \ldots 4f^{3}5s^{2}5p^{6}$$

The different energy states of an atom are usually labelled by symbols of the form, $^{2S+1}L_J$, where S is the total spin quantum number, L is the total orbital quantum number (0, 1, 2, 3, 4, 5, values that are expressed by capital letters S, P, D, F, G, H, I) and J the total angular momentum obtained by combination of L and S.

Ce^{3+} contains only one electron in the 4f shell and thus few energy levels. This results in two different states in the 4f shell from which electrons promote to the conduction band as shown in Fig. 1 [18]. The transition to the least energetic level of the conduction band depends on the host material where the ion is located, taking place under 370 nm excitation in borate glasses and under 500 nm in YAG ceramics [19]. It presents a broad emission band centered around 470-550 nm that also depends on the host material.

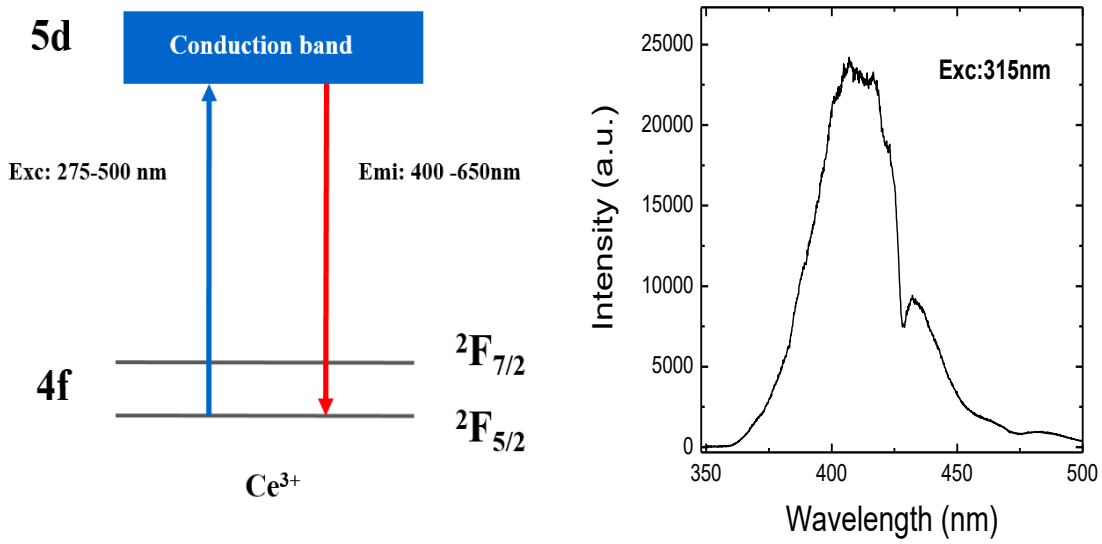

Figure 1. (Left) Schematic energy level diagram of Ce^{3+} indicating the transitions between the valence and the conduction band. (Right) Emission spectra of Ce^{3+} ions in a glass sample codoped with Ce^{3+} and Nd^{3+}.

The Nd^{3+} energy level distribution presents very close energy levels to its ground state, $^4I_{9/2}$. A high energy gap separates these states from the $^4F_{3/2}$ electronic excited state. The following levels are close to each other and their distribution does not present other large energy gaps. The $^4F_{3/2}$ level is thermally coupled to the $^4F_{5/2}$ level. This means that as temperature rises the atoms on the $^4F_{3/2}$ level promote to the $^4F_{5/2}$ level by thermal redistribution.

When Nd^{3+} is excited under visible light, the atoms are promoted to high energy levels. A small portion of atoms can return to the ground state by radiative transitions, but most of them quickly decay to the $^4F_{3/2}$ level by non radiative mechanisms, as a result of the small energy difference between these levels. Due to the large energy gap, the probability of non radiative transitions is quite small and the de-excitation is carried out by photon emission to the lower energetic levels as seen in Fig. 2 (left). If after photon emission the atom does not decay to the ground state, it finally reaches it by non radiative transitions. All these transitions lead to an emission spectrum like the one shown in Fig. 2 (right).

The Nd^{3+} 1064 nm emission from the $^4F_{3/2} \rightarrow {}^4I_{11/2}$ transition can produce laser emission. This takes place when population inversion occurs, i.e. the number of ions in the $^4F_{3/2}$ level is greater than in the $^4I_{11/2}$ level, and the resonator internal gain is greater than the passive losses.

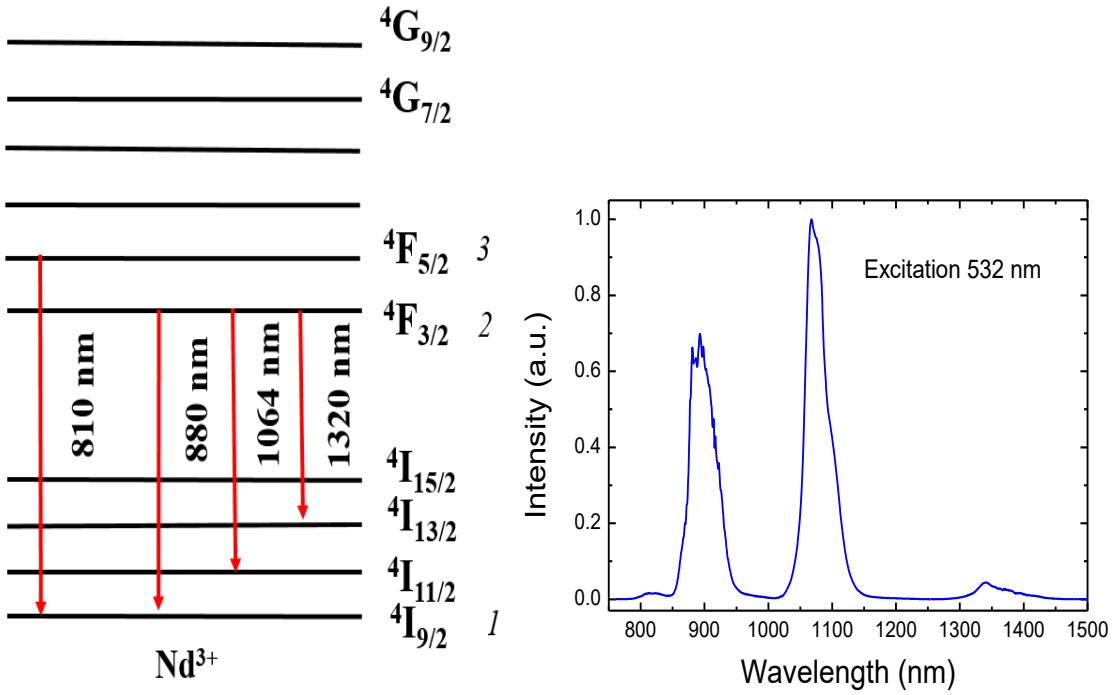

Figure 2. (Left) Schematic energy level diagram of Nd^{3+} ions indicating the near infrared emissions obtained under visible excitation. (Right) Emission spectra of Nd^{3+} ions located inside a glass under 532 nm excitation.

Photon upconversion

Photon Upconversion (UC) is the process where the absorption of two or more photons produces the emission of a photon with shorter wavelength than the wavelength of the excitation photons. Upconversion emission from high excited levels of lanthanide ions can be obtained mainly via two distinct mechanisms: energy transfer upconversion (ETU) and excited state absorption (ESA) [20]. ESA consists on the absorption of two or more photons by a single atom while ETU involves the absorption of photons by different atoms, giving rise to an atom in a higher energy state by non radiative energy transfer between these ions as shown in Fig. 3 (right).

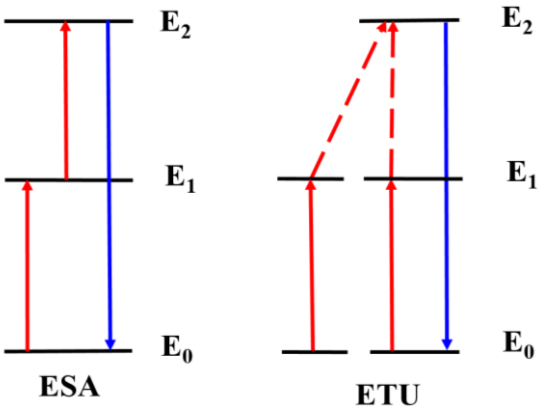

Figure 3. Schematic diagrams of ESA and ETU upconversion mechanisms.

Considering a three level system (see Fig. 3), the model that describes the ETU upconversion mechanism is based in the following rate equations

$$\frac{dN_1}{dt} = \sigma\phi A - \frac{1}{\tau_1}N_1 - 2W_{up}N_1^2 \quad (1)$$

$$\frac{dN_2}{dt} = -\frac{1}{\tau_2}N_2 + W_{up}N_1^2 \quad (2)$$

where σ is the absorption cross-section, ϕ is the incident pumping flux, A is the concentration of ions, τ_1 and τ_2 are the mean lifetime of excited states 1 and 2, N_1 and N_2 are the number of atoms in the states 1 and 2, and W_{up} is the probability that photon upconversion occurs.

Under stationary regime, these equations can be solved neglecting the upconversion term in Eq. (1), since W_{up} is small compared to the other terms. This approximation is valid in experiments with low excitation intensities. In this situation, the population of level 2 is given by:

$$N_2 = W_{up}\tau_2(\tau_1\sigma\phi A)^2 \quad (3)$$

Taking into account that the intensity of the emission of these levels may be expressed as:

$$I_i = N_i h\nu_i A_{i1} \qquad i=3,\ 2 \quad (4)$$

where A_{i1} is the spontaneous emission rate from the ith level, then, a plot in a logarithmic scale of the intensity of upconversion emission, I_2, as a function of the excitation intensity, I_{Exc}, yields a straight line of slope 2. In general, for an upconversion process involving n photons, a straight line of slope n is obtained.

When upconversion emission is observed it is possible to determine which mechanism is taking place by studying the temporal evolution of the emission under pulsed excitation in the near infrared. Considering a three level system as above, with no external radiation, the rate equations for the population of levels 1 and 2 in the case of ETU process can be expressed as:

$$\frac{dN_1}{dt} = -\frac{1}{\tau_1}N_1 - 2W_{up}N_1^2 \quad (5)$$

$$\frac{dN_2}{dt} = -\frac{1}{\tau_2}N_2 + W_{up}N_1^2 \quad (6)$$

Taking into account in Eq. (5) that the W_{up} probability is small compared to $1/\tau_1$ and that at time, t=0, the number of excited atoms in the level 1 is N_0, the solution from equation (5) is given by:

$$N_1(t) = N_0 exp\left(-\frac{t}{\tau_1}\right) \tag{7}$$

Introducing Eq. (7) into Eq. (6):

$$\frac{dN_2}{dt} = -\frac{1}{\tau_2}N_2 + W_{up}N_0^2 exp\left(-\frac{t}{\tau_1/2}\right) \tag{8}$$

This differential equation of first order can be solved applying an integrating factor, and the solution is:

$$N_2(t) = Bexp\left(-\frac{t}{\tau_2}\right) + \frac{W_{up}N_0^2}{\frac{1}{\tau_2}-\frac{t}{\tau_1/2}} exp\left(-\frac{t}{\tau_1/2}\right) \tag{9}$$

Using the condition that at t=0 the level 2 is not populated $N_2(0)=0$, then Eq. (9) is rewritten as:

$$N_2(t) = \frac{W_{up}N_0^2}{\frac{1}{\tau_2}-\frac{t}{\tau_1/2}} \left(exp\left(-\frac{t}{\tau_1/2}\right) - exp\left(-\frac{t}{\tau_2}\right)\right) \tag{10}$$

This result shows that by ETU process, the population of level 2 increases, when there is no external radiation, from the atoms at level 1 and slowly decreases once the maximum is reached. Then, the temporal evolution of upconverted emission produced by ETU can be expressed as:

$$I_2(t) = \frac{W_{up}N_0^2 h\nu_2 A_{20}}{\frac{1}{\tau_2}-\frac{t}{\tau_1/2}} \left(exp\left(-\frac{t}{\tau_1/2}\right) - exp\left(-\frac{t}{\tau_2}\right)\right) \tag{11}$$

If the upconversion is obtained by ESA, the intensity of the emission quickly decays when there is no external radiation and the temporal evolution can be expressed by a decreasing exponential like Eq. (7):

$$I_2(t) = I_0 exp\left(-\frac{t}{\tau_2}\right) \tag{12}$$

where I_0 is the maximum of the intensity at t=0.

Finally, if both mechanism take action, the temporal evolution of the emission will be a combination of both processes.

Energy transfer processes

The intensity of the emission from a sample doped with optically active ions depends on the concentration of the dopant. At low concentrations the emission will intensify as the dopant concentration increases. However, at high concentrations this trend reverses and the emission decreases as the concentration of the dopant increases. This is due to the fact that the mean distance between the active ions decreases as their number in the host material rises. This leads

to an increase of energy transfer processes between those ions and a significative reduction of the intensity of the emission.

If the sample is exposed to pulsed excitation and it is assumed that non radiative energy transfer processes, with no photons involved are taking place, multipolar interaction between the ions is the predominant interaction and the migration among donors is not relevant. In this case the temporal evolution of the emission follows the Inokuti-Hirayama model [21].

$$I(t) = I_0 exp\left(-\frac{t}{\tau} - Q\left(\frac{t}{\tau}\right)^{3/s}\right) \quad (13)$$

where I_0 is the intensity at time t=0; τ is the intrinsic lifetime of the engaged donor level; S is equal to 6,8 or 10 depending on the type of interaction (for dipole-dipole interaction, S=6) and, if there is only one type of acceptor ion, Q is given by:

$$Q = \frac{4\pi}{3}\Gamma\left(1 - \frac{3}{S}\right) A(C_{DA}\tau)^{3/S} \quad (14)$$

where Γ is the gamma function, A is the concentration of ions and C_{DA} is the donor-acceptor energy transfer parameter.

All the samples analysed present the same concentration of rare earth ions and the intensity of the emission cannot be studied as a function of the concentration. Nonetheless, the temporal evolution of the emission will be fitted to Eq. (13) and to a decaying exponential function to determine if energy transfer processes are occurring inside the material.

Fluorescence Intensity Ratio (FIR)

The FIR technique is based on the variation of the relative luminiscense of two radiative transitions with temperature. This technique allows to perform a calibration that can be used to estimate the temperature of a given sample from its emission spectrum.

Not all the possible transitions of an element are appropriate to apply the FIR technique. If the energy difference is larger than 2000 cm^{-1}, the upper level population would be extremely low because the thermal energy (~k_BT) cannot promote electrons from one level to another. On the contrary, if the energy is lower than 200 cm^{-1} the emission from each level would be overlapped and would make it difficult to apply this technique [15].

In summary, only energy levels with an energy gap between 200 cm^{-1} and 2000 cm^{-1} and close to the thermal energy associated with the range of temperatures to be measured, are good candidates for this technique. An important consequence of this behaviour is that the ratio of the intensities is not affected by the pump power of the incident source.

For a three level system , labelled 1, 2 and 3, in thermal equilibrium, the relative population of the levels energetically close, labelled 2 and 3 (see Fig. 2(left)), follows a Boltzmann type distribution. Accordingly, the ratio of the intensities from these levels, is given by [10, 12]:

$$R = \frac{I_{31}}{I_{21}} = \frac{A_{31} g_3 h\nu_3}{A_{21} g_2 h\nu_2} exp\left(\frac{-E_{32}}{K_B T}\right) = B\ exp\left(\frac{-E_{32}}{K_B T}\right) \quad (15)$$

where, g_3 and g_2 are the degeneracies (2J+1) of the levels, E_{32} is the energy gap between the two levels and K_B is the Boltzmann constant.

Whispering Gallery Modes (WGM)

The theoretical study of WGM resonances can be addressed by using different approaches [22]. One of them, analyses the resonances inside a microsphere by solving the Helmholtz wave equation in spherical coordinates. Under the assumption that the microsphere is a homogeneous dielectric sphere, the solution for the intensity distributions can be expressed in terms of eigenfunctions for the radial, azimuthal and polar coordinates [23]. Each of these eigenfunctions are associated with the radial, polar and azimuthal mode numbers, n, l and m respectively. The radial mode number n gives the number of nodes of the intensity distribution in the radial direction. The polar mode number l is approximately the number of wavelengths packed along the circumference of the resonator travelling along the equator of the sphere. For each polar mode number l, the allowed m values are in the range of –l<m<l, leading to a 2l+1 degeneracy of the azimuthal modes.

There is also a geometrical optics approach that even though its simplicity gives a quick explanation of the physical phenomenon [24]. In this model, the light circles the interior of the sphere through multiple total internal reflections returning in phase to the origin point. The resonance condition of a given wavelength λ inside of a microsphere of radius R>> λ is approximately described by the following equation:

$$2\pi\, n\, R = l\lambda \quad (16)$$

where *l* is the polar mode number and n is the index of refraction of the sphere.

Eq. (16) allows to evaluate WGM resonances inside the sphere taking into account only the sphere parameters. However, each time the light is reflected it experiences small phase differences. These differences depend on the wavelength, the light angle of incidence and the surrounding media to sphere refractive index ratio. Therefore, the total optical path length is slightly different from 2πnR and must be taken into account to perform a more accurate calculus.

Small perturbations in shape, size, or refractive index of the sphere cause a shift in the resonant wavelength. This allows to estimate the external conditions of the microsphere causing the difference in its properties. These changes on the parameters of the microsphere can be produced by variations in pressure, chemical composition of the surrounding media or temperature. In order to know the relationship of the resonant wavelength with temperature, the derivative of Eq. (16) is calculated:

$$\frac{d\lambda}{dT} = \lambda\left(\frac{1}{n}\frac{\delta n}{\delta T} + \frac{1}{R}\frac{\delta R}{\delta T}\right) = (\alpha + \beta)\lambda \quad (17)$$

where α is with the thermo-optic coefficient (α= 1/n δn/δT) and β the thermal expansion coefficient (β=1/R δR/δT). The sign of these coefficients is known to be generally positive in glasses [25]. Therefore, it is concluded that the peaks will shift to the red region of the spectra as the temperature increases. As example, Fig. 4 shows the red shift of a WGM peak at different temperatures as explained before.

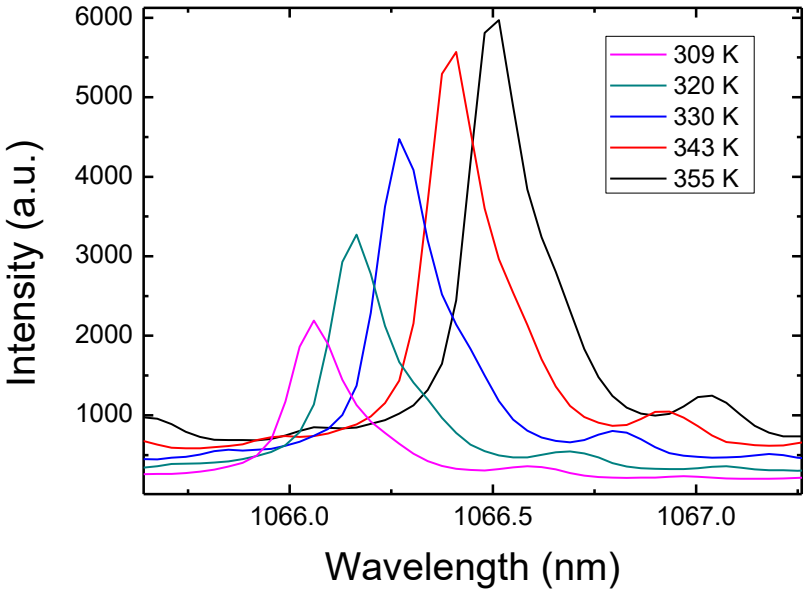

Figure 4. Wavelength displacement of a WGM resonance at different temperatures in the emission spectrum of Nd^{3+}.

Thermal Sensors

FIR technique and WGM displacement are techniques that can be used to developed thermal sensors. In order to characterise the performance of a thermal sensor two parameters need to be introduced: sensitivity and resolution. The sensitivity, S, represents the variation of the measured parameter, MP, with temperature relative to its magnitude.

$$S = \frac{1}{MP}\frac{dMP}{dT} \tag{18}$$

According to this definition, it is straightforward to calculate the sensitivity for the aforementioned methods, the FIR technique and the WGM, using Eqs. (14, 16), giving as a result the following expressions:

$$S_{FIR} = \frac{1}{R}\frac{dR}{dT} = \frac{E_{32}}{K_B T^2} \tag{19}$$

$$S_{WGM} = \frac{1}{\lambda}\frac{d\lambda}{dT} = \left(\frac{1}{n}\frac{\delta n}{\delta T} + \frac{1}{R}\frac{\delta R}{\delta T}\right) = \alpha + \beta \tag{20}$$

Eq. (19) must be carefully analysed because it can lead to misinterpretations. It suggests that using pairs of energy levels with larger energy differences the FIR sensitivity increases, but for large energy differences, the energy levels have no temperature correlation and this technique is not valid as explained before. It also indicates that the sensibility enhances at low temperatures,

but this implies extremely low upper level populations, corresponding to excessively low emission and so, the ratio of intensities is determined with undesirable uncertainty.

In addition, the temperature resolution of the FIR technique and WGM can be estimated taking into account the resolution of the instrument and the temperature sensitivity of the technique [26]:

$$\Delta T_{\min FIR} = \frac{\Delta R}{R\, S_{FIR}} \tag{21}$$

$$\Delta T_{\min WGM} = \frac{\Delta \lambda_{min}}{\lambda\, S_{WGM}} \tag{22}$$

Eqs. (21, 22) show that the temperature resolution of both techniques is greater for larger values of the sensitivity.

Experimental Methods

In this section the experimental devices and methods used in this work will be described. They can be arranged in three main different parts. The first one is the microsphere fabrications. The second stage comprises the thermal calibration of the bulk sample. It is performed to know how the ratio of intensities from thermally coupled levels varies with temperature. In this way, the temperature of the sample can be inferred by obtaining its emission spectrum. The final part includes set-ups used to perform the optical measurements to characterise the material.

Microsphere production

The most extended method to produce microspheres is the rapid quenching of liquids droplets [27]. This consist on melting small glass particles from a bulk sample and allowing surface tension to pull the molten glass into a sphere that is rapidly quenched. There are some complementary steps like chemical etching, which are normally used in order to polish the microsphere surface and obtain high sphericity values [28].

The microspheres used in this experiment were produced by Prof. Vladimir N. Sigaev from D. I. Mendeleev Russian Chemical Technology University. They have been obtained from a codoped Ce^{3+} and Nd^{3+} YAS glass (YAS: Ce^{3+}–Nd^{3+}) with the following composition (mol %): 13.4 Y_2O_3, 37.2 AlO_3, 46.5 SiO_2, 0.3 Ce and 2.6 Nd by the melt quenching method in a platinum crucible. The bulk glass sample is reduced to small particles and separated attending to grain size by wet sieving. The powder is then exposed to plasma that gives them their spherical shape [29].

Temperature Calibration

The emission spectrum response to temperature of the YAS: Ce^{3+}–Nd^{3+} codoped glass was obtained by the Grupo de Espectroscopía Láser y Altas Presiones from La Universidad de La Laguna. The experimental set-up is shown in Fig. 5. The sample is located inside a tubular horizontal furnace where the excitation of the Nd^{3+}ions is carried out with a 532 nm continuous wave Nd:YAG laser at the minimum power to avoid optically heating the sample. This laser is focalised with a lens on the sample and impinges it from one side of the furnace. The luminescence from the sample was focalized at the tip of an optical fiber located in the opposite side of the furnace with the help of one collimating and one focusing lens. The optical fiber was coupled to a single grating CCD spectrometer (Andor SR-3031-B CCD Newton DU920N). The heating of the sample was performed at a rate of 1 K min^{-1} from room temperature to 473 K and was monitored with a thermocouple connected to a digital multimeter and located very close to the sample without touching it. The recorded spectra were corrected from the instrumental response.

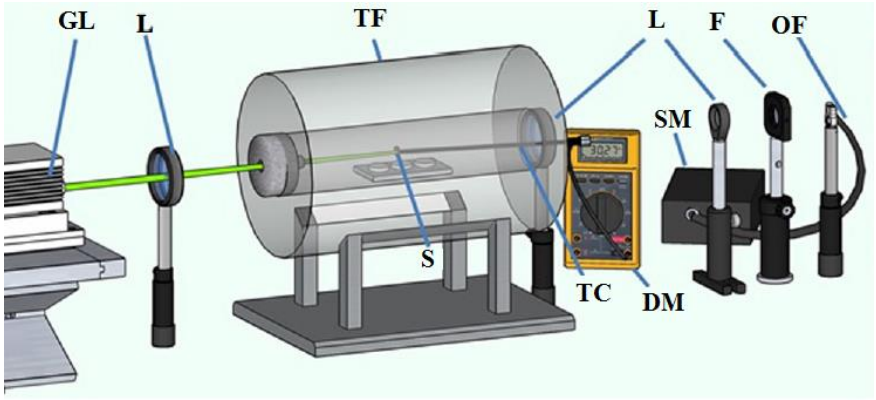

Figure 5. Experimental set-up employed for the temperature calibration of the Nd^{3+} emission. The acronym labels correspond to GL Green Laser, L Lens, TF Tubular Furnace, S Sample, TC thermocouple, DM Digital Multimeter, F Filter, OF Optical Fiber and SM Spectrometer [8]

Optical Measurements

The emission spectra of YAS: Ce^{3+}–Nd^{3+} microspheres were measured using two different set-ups. In both of them microspheres were handled and supported by means of a needle and the ensemble was located on an XYZ translational stage that moves independently from the rest of the device. An aligned configuration was used to excite and detect the microspheres luminescence. The sample was always located at the focal plane of a 20 x microscope objective.

In the first set-up, shown on Fig. 6, a continuous wave 532 nm Nd:YAG laser was used to excite the Nd^{3+} ions in the microsphere. The green laser light from the excitation source comes from Nd^{3+} ions inside a YAG crystal that forms the active medium optically pumped by a laser diode in the resonant cavity. Finally, the Nd:YAG green line is filtered from the diode pumping laser by a 560 nm short pass filter. The light goes through a small pinhole and a collimating lens to obtain a circular collimated bean. A dichroic mirror is used to reflect the incident beam towards the microscope objective that focalizes the light into the centre of the microsphere. A beam splitter that redirects part of the light to a CCD camera is located between the dichroic mirror and the microscope objective. This camera shows a real time image of the microspheres on a television screen, enabling to track microsphere position thanks to a LED white source located behind the sample. The transmitted light was filtered from the excitation source by a 590 nm long pass filter to avoid second harmonics and focused in the entrance slit of an Andor CCD spectrograph (Andor Newton SR-3031-B CCD Newton DU920N) after being reflected by a high precision mirror. This mirror can be replaced by an optical fiber when another instrument is used.

The excitation and detection zones of the WGM resonances are critical. To optimize the data acquisition, the centre of the microsphere is chosen as the excitation zone and the border as the detection zone [9]. The selection of the excitation area is performed by means of the XYZ

translational stage with the aid of the television screen images while the detection region is selected with the high precision mirror and closing the spectrograph slits to 50 μm.

Due to the lack of sensitivity of the silicon CCD detector beyond 1100 nm, the microsphere emission was guided to a second spectrometer (ANDOR SR-500i-B2 InGaAs CCDDU490A-1.7) equipped with an optical fiber to measure the 1300 nm band. Both recorded spectra were corrected from the instrumental response.

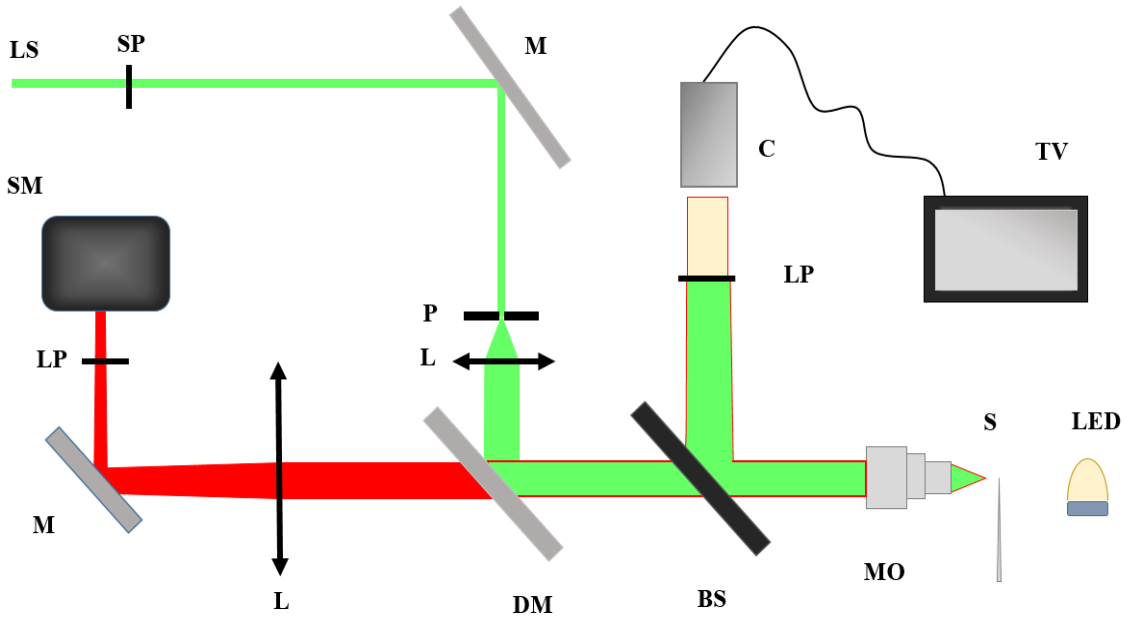

Figure 6. Experimental set-up used to measure WGM and laser emission. The acronym labels correspond to LS Laser source (532 nm), SP Short pass filter, LP Long Pass filter M Mirror, SM Spectrometer, P Pinhole, DM Dichroic mirror, L Lens, BS Bean splitter, C camera, TV Television screen, MO Microscope objective, S Sample and LED white light source.

In order to study the upconversion process the excitation source was replaced by a continuous wave titatium:saphire laser tuned at 808 nm pumped by a Nd:YAG continuous laser as shown on Fig. 7. The wavelength of the laser is first manually selected and then filtered by 750 nm long pass filter for the same reasons shown in the previous set-up. The laser beam is focused in the centre of the microsphere by a lens and the emitted light is collected by the microscope objective. The upconversion emissions is filtered from the laser light by a 750 nm short pass filter and focused in the entry slit of the spectrograph.

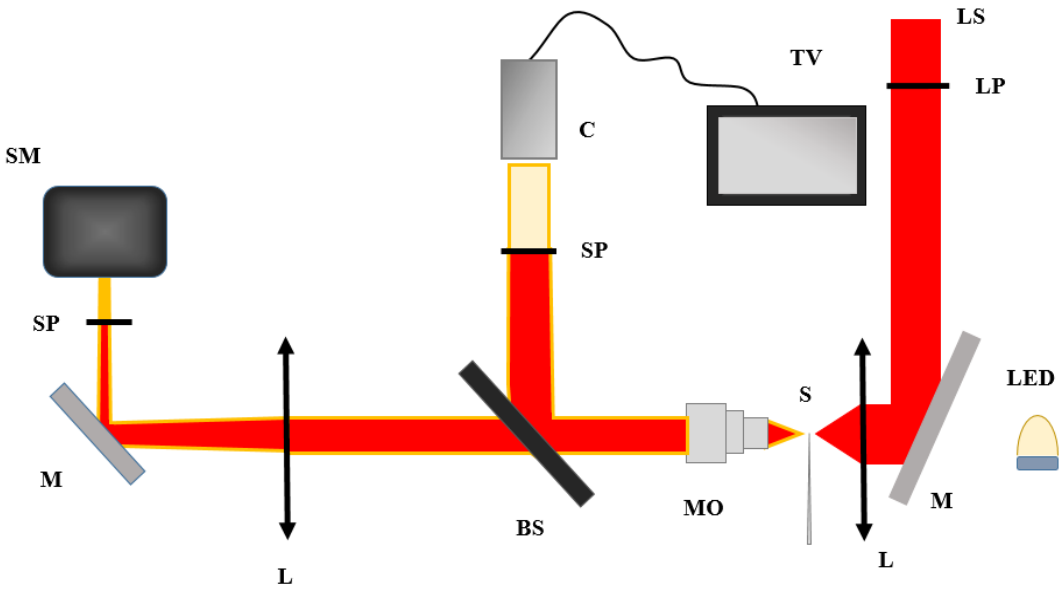

Figure 7. Experimental set-up used to measure upconversion emission. The acronym labels correspond to LS Laser source (808 nm), SP Short pass filter, LP Long pass filter, M Mirror, SM Spectrometer, L Lens, BS Bean splitter, C camera, TV Television screen, MO Microscope objective, S Sample and LED white light source.

Microspheres with a diameter between 30 and 50 μm were studied. The spectra showing WGM were recorded for increasing values of the laser pumping power to study the microsphere laser emission, WGM peak shift and upconversion emission. All the spectra were corrected from the instrumental response.

Measurement of the temporal evolution of the luminescence have been carried out for optical characterization of the processes occurring in the material. The bulk glass sample was excited with the emission from an optical parametric oscillator laser that provides 10 ns pulses at 10 Hz repetition rate. The emission of the sample is focused in the entry slit of a Triax 180 monochromator, and detected with a coupled photomultiplier specific for visible measures. The luminescence of the sample was filtered by a long pass filters to avoid the laser source entering the detector. A digital oscilloscope TEKTRONIX-2430A was used to register the signal. Ce^{3+} ions present very short lifetime and to study their emission a commercial Edinburgh Instruments LifeSpec II was employed due to its greater time resolution compared to the oscilloscope which is limited to 25ns with a 50 Ω input resistance.

The absorption spectrum of the bulk sample of YAS: Ce^{3+}–Nd^{3+} glass in the range from 200 to 1000 nm was measured with the spectrophotometer Cary 5000 to obtain the value of the energy gap between the thermally coupled levels of neodymium, E_{32}.

Results and discussion

The results obtained in the experiments described in the previous section are presented in this section. The first subsection shows the result from the temperature calibration of the bulk sample. The second one comprises the emission spectrum from the microspheres and the WGM dependence with temperature. The next subsection presents the results of the laser emission. The following subsection involves the upconversion emission measurements and the final part analyses the intensity decay measurements of different levels in order to understand the dynamic of the processes involved.

Temperature calibration

The $^4F_{5/2}$ and $^4F_{3/2}$ energy levels of Nd^{3+} ions are very close to each other. Therefore the $^4F_{5/2} \rightarrow {}^4I_{9/2}$ (810 nm) and $^4F_{3/2} \rightarrow {}^4I_{9/2}$ (880 nm) transitions are thermally coupled and their populations follow a Boltzmann distribution law. Hence, the ratio of the intensities of these emissions follows the temperature dependence given by Eq. (15).

The experimental values obtained for the intensity ratio are plotted in Fig. 8 (left) and fitted to Eq. (15) obtaining a value of 956 cm^{-1} for the energy gap E_{32} and a pre-exponential parameter B with a value of 2.85. The value for the energy gap is similar to the value of 1053 cm^{-1} obtained from absorption spectrum in Fig. 8 (right). This value was estimated by calculating the energy difference between the maximums of each band.

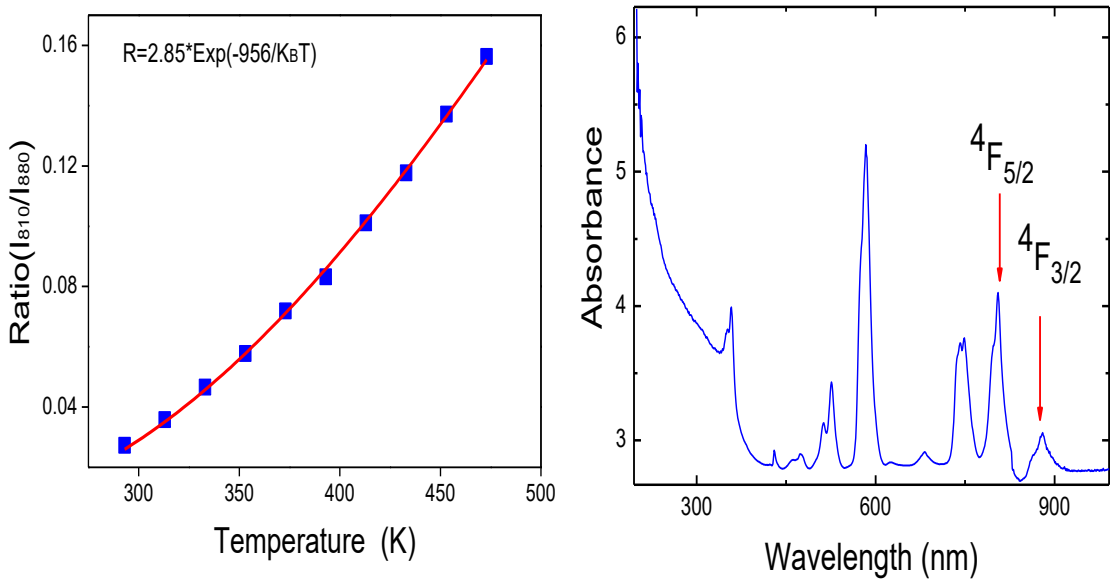

Figure 8. (Left) Experimental values of the ratio of the intensities between the thermalized bands of Nd^{3+} obtained from the bulk sample inside an electrical furnace (blue squares) and fitted curve to Eq. (15) (solid red line). (Right) Absorption spectrum of the bulk sample. The absorption peaks used to obtain the energy gap are marked with red arrows.

Using this calibration, the temperature of the microspheres will be obtained in the incoming results by calculating the ratio of the intensities of the emission bands from the thermally coupled levels. This is possible because the microspheres are made of the same material than the bulk sample used for the temperature calibration and hence the emission band of Nd^{3+} ions in the microspheres will present the same changes with temperature.

In order to characterize the performance of the FIR technique, the sensitivity is calculated applying Eq. (19) and plotted in Fig. 9.

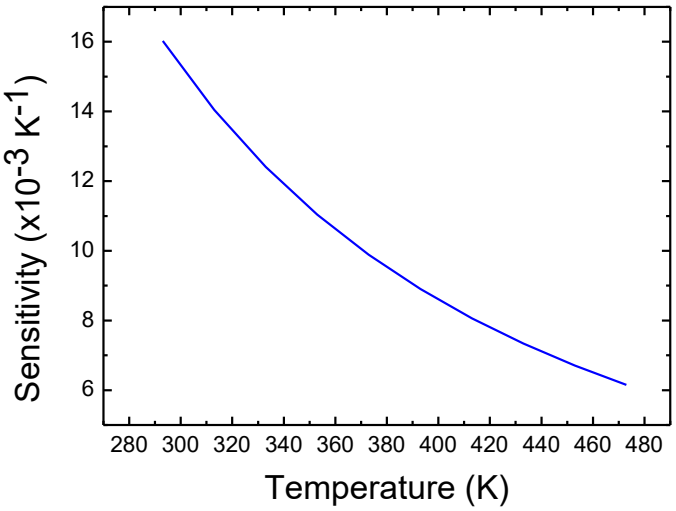

Figure 9. Sensitivity of the FIR technique calculated using Eq. (19).

It can be seen that it achieves its maximum value (S_{FIR}=1.60 $\cdot 10^{-2}$ K^{-1}) at the lowest temperature in the measured range. This yields to a temperature resolution of the order of 3 K using Eq. (21) if an error of 5% in the calculation of the ratio is assumed. This error is due to the inaccuracy of the areas due to the overlap between the thermalized bands.

Displacement of the WGM

When the Ce^{3+}-Nd^{3+} codoped YAS glass is excited under 532 nm laser action, the spectrum plotted in Fig. 2 (right) is obtained. These transitions correspond to the radiative emissions from the $^4F_{3/2}$ and $^4F_{5/2}$ to the less energetic levels.

A similar spectrum is obtained when a microsphere is made out of the same material and exposed under the same radiation. However, if the excitation is carried out in the centre of the microsphere and the detection is located near its border, sharp peaks appear due to the WGM resonances as mentioned above. Fig. 10 shows the complete emission spectrum of Nd^{3+} ions with the narrow peaks from the WGM resonances. In this spectrum the $^4F_{5/2} \rightarrow {}^4I_{9/2}$ (810 m) and $^4F_{3/2} \rightarrow {}^4I_{9/2}$ (890 nm) transitions used for the thermal calibration, the $^4F_{3/2} \rightarrow {}^4I_{11/2}$ transition (1064 nm) and the $^4F_{3/2} \rightarrow {}^4I_{13/2}$ transition (1320 nm) are shown.

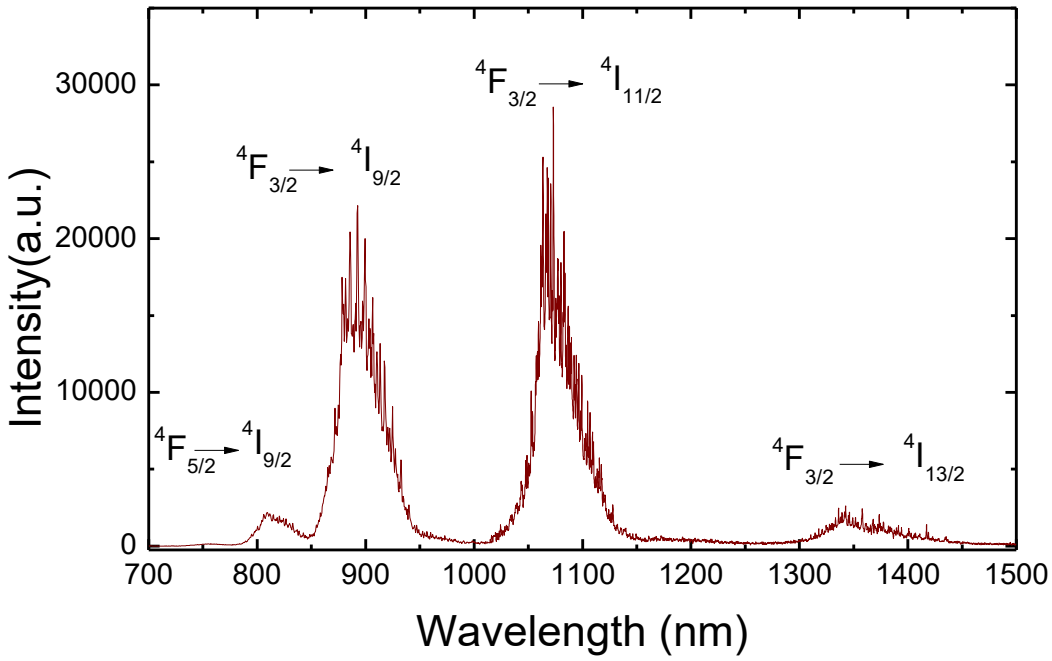

Figure 10. Spectra showing the Whispering Gallery Modes overlapped with the neodymium emission under 532 nm laser excitation and 119 mw pump power.

The emission spectrum shown in Fig. 10 was obtained for different laser powers. As a consequence, two different effects related with the laser heating of the microsphere were observed. The first one is the difference of the ratio of the intensities from the $^4F_{5/2}$ and the $^4F_{3/2}$ emissions due to the thermal redistribution of population. This enables to obtain the temperature of the microsphere using the thermal calibration performed to the bulk sample, under the assumption that the WGM resonances do not affect the overall shape of the emission band.

The second one is the displacement of the WGM wavelength to the red region of the spectra. Thereby, it can be performed a study of the displacement of the WGM as a function of temperature. If the dependence of the index of refraction with temperature is neglected the shift of the resonances can be explained as follows. Due to laser heating, the volume of the sphere increases and, as a consequence of the shift in the dimensions of the resonator cavity, the wavelengths of the WGMs change according to Eq. (17). Therefore, a linear red shift of the wavelength of the WGM is expected, as shown in Fig. 11.

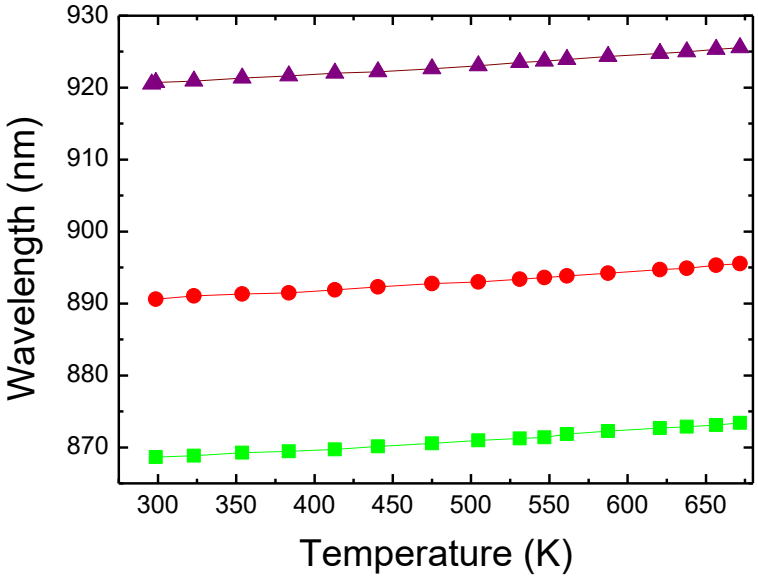

Figure 11. Displacement of three WGM peaks as a function of temperature.

From the measurements of the wavelength displacements corresponding to the maxima of three WGM resonances, plotted in Fig. 11, an average displacement of 12.9 pm/K was obtained. It has been found that higher values of the shifts were obtained for the peaks in the 1300 nm band. This behaviour can be deduced from Eq. (17). Fig. 12 shows the values of the slope of WGM resonances at different wavelengths. It seems that there is a linear dependence between the slope and the wavelength of the WGM resonance (in good agreement with Eq. (17)).

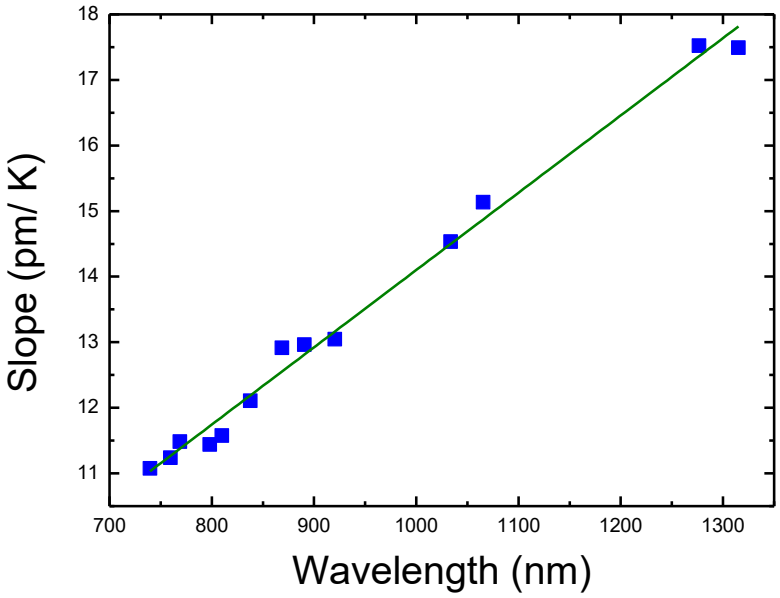

Figure 12. Displacement of the WGM resonances with temperature for different values of the wavelength WGM resonance (blue squares). Guide line (green solid line).

To compare this method with the FIR technique, the sensitivity of the wavelength displacement was calculated under the assumption that the wavelength is a linear function of temperature. As example, Fig. 13 shows the sensitivity values obtained for two different wavelengths corresponding to the maximum and the minimum values of the shift from Fig. 12.

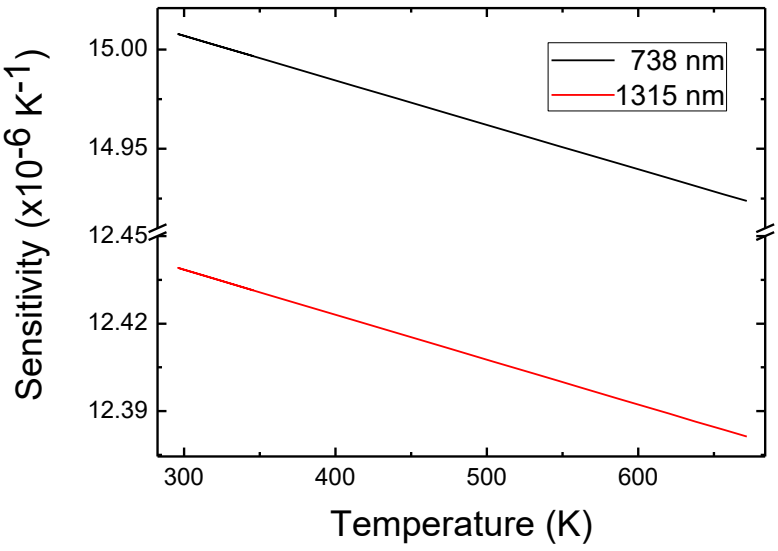

Figure 13. Sensitivity for the displacement of two WGM resonances using Eq. (20). The WGM at these wavelengths present the maximum and minimum values of the shifts from Fig. 12.

The sensitivity of the displacement of the WGM reaches its maximum value ($S_{WGM}=15\cdot10^{-6}$ K^{-1}) for the shorter wavelength at the lowest temperature in the measured range in a similar way to S_{FIR}.

The WGM limit of resolution of the resonant wavelength is about 1% of its line-width [30-31]. The narrowest line-width observed in the emission spectra of the microspheres was about 0.3 nm in the 1300 nm band. Using these values in Eq. (22) the temperature resolution is the order of 0.2 K. Therefore the resolution in the WGM technique is one order of magnitude more accurate than the FIR technique.

Laser emission

Another consequence of the continuous reflections of light inside the walls of the microsphere is that if it is doped with an optically active material, it can act like a conventional resonant cavity and produce laser emission.

The microspheres studied in this work contain neodymium ions capable to produce laser emission. Neodymium can be studied as a four level system because it presents two non radiative and one radiative transition in the $^4F_{5/2}\rightarrow{}^4F_{3/2}\rightarrow{}^4I_{11/2}\rightarrow{}^4I_{9/2}$ de-excitation process.

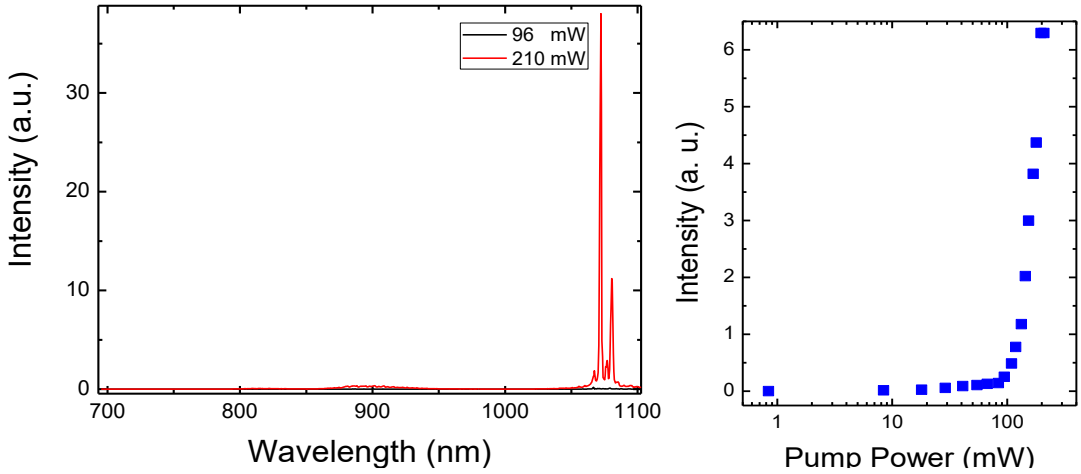

Figure 14. (Left) Emission spectra of a YAS: Ce^{3+}–Nd^{3+} microsphere at pump powers below the laser threshold (black line) and above threshold (red line). (Right) Intensity of the 1072 laser emission at different pump powers.

Fig. 14 (left) presents the emission spectrum of Nd^{3+} ions in a microsphere at different pump powers, showing the multimode laser region at the 1064 nm band. By analysing the behaviour of the most intense peak (1072 nm) as a function of the pumping power (shown on Fig. 14 (right)) the laser threshold power is calculated, obtaining a value of 100 mW.

It is possible to reduce the laser threshold by changing the wavelength of the pumping laser to 808 nm. Neodymium ions absorb more efficiently this wavelength than the 532 nm employed,

as can be inferred from the higher value for the absorbance at 808 nm. Moreover, the 808 nm radiation directly connects the $^4I_{9/2}$ and $^4F_{5/2}$ levels, decreasing the losses due to non radiative de-excitation mechanisms. Hence, lower values of the laser threshold are expected.

Others authors, using a different type of microsphere [32], have found that the laser threshold decreases about an order of magnitude by adding a mechanical chopper to the pump laser. This is because on average, the microsphere receives less power with the chopped pump than under continuous wave pump and as a result the microsphere cools down.

Upconversion

The microspheres were excited with a continuous wave 808 nm laser in the set-up described in Fig. 7. As shown in Fig. 15, the emission spectra presents shorter wavelength than the excitation source, what means that upconversion processes are taking place inside the microsphere. The narrow peaks in the spectrum are the WGM resonances that are a consequence of total reflection of light inside the surface of the microsphere.

The emission bands can be identified with the transitions from the high energy levels in Fig. 2 (left). The first three bands correspond to transitions from the $^4G_{7/2}$ level to the $^4I_{9/2}$, $^4I_{11/2}$ and $^4I_{13/2}$ levels, respectively. In the region of 700 nm, the $^4G_{7/2} \rightarrow {}^4I_{13/2}$ emission band is overlapped with the $^4F_{9/2} \rightarrow {}^4I_{9/2}$ emission band. The last emission band correspond to the $^4F_{7/2} \rightarrow {}^4I_{9/2}$ and is cut due to the presence of the shortpass filter that blocks the light with wavelength larger than 750 nm. These last two bands increase their intensity at higher rates than the shorter wavelength bands. This shows that these levels are not being populated by the same mechanisms than the other bands. Attending to the increase of intensity with the pumping power, it is observed that these bands are being populated by thermal redistribution mechanisms following a Boltzmann distribution as it's been shown in the latter section.

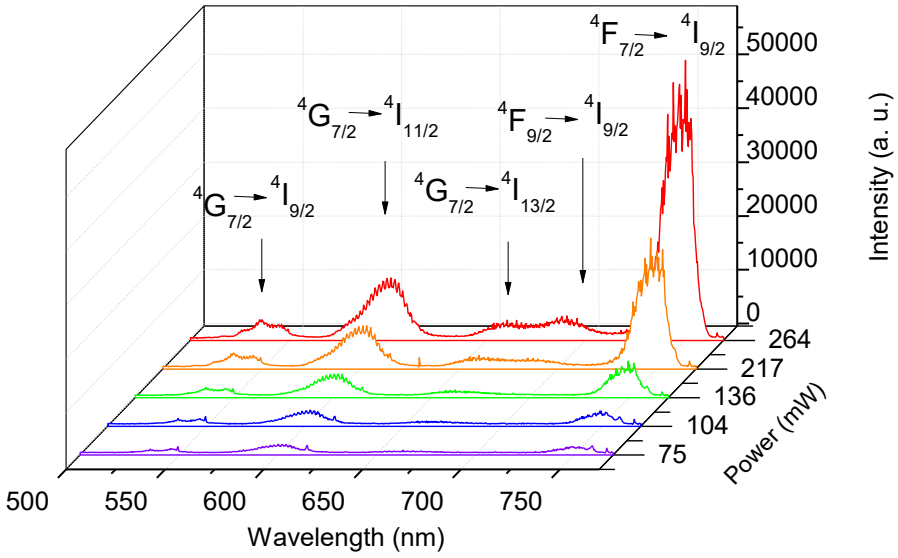

Figure 15. Upconversion emission spectra from Nd^{3+} ions inside a microsphere obtained at different pump powers. WGM resonances appear superimposed to these emissions.

A plot of the intensity of the upconverted emission as a function of the intensity of the excitation source in a logarithmic scale should yields a straight line with slope n, with n the number of photons involved in the process. This plot for the $^4G_{7/2} \rightarrow {}^4I_{11/2}$ emission band is shown in Fig. 16 where a value of 1.6 has been obtained for the slope. This result indicates that two infrared photons of 808 nm wavelength are required to produce the upconversion emission.

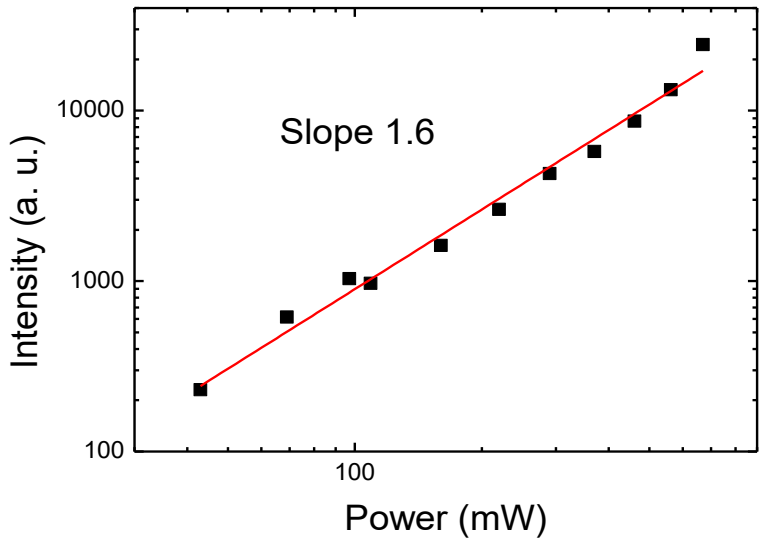

Figure 16. Dependence of the upconversion emission at 579 nm with the excitation power of 808 nm.

WGM on the visible region of the spectrum shown in Fig. 15 present the same behaviour than the WGM studied in the latter section. They experience a wavelength red shift when the

temperature of the sample increases as shown in Fig. 17. However, there is no calibration for the thermally coupled levels on this region of the spectrum and the FIR technique cannot be applied. Consequently, the temperature of the microsphere is a non accessible parameter.

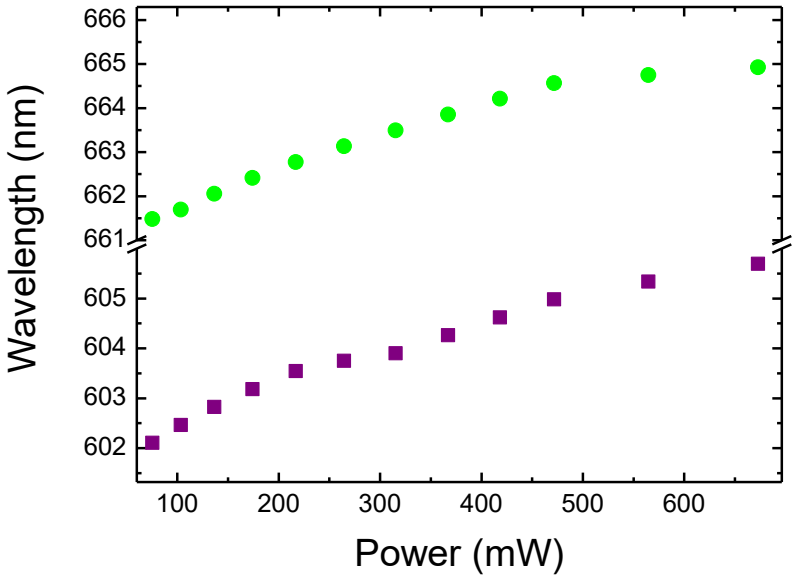

Figure 17. Displacement of two WGM peaks as a function of the incident pump power.

Time resolved experiments

Time resolved experiments have been performed in an attempt to determine if non radiative energy transfer processes are taking place.

The temporal evolution of $^4F_{3/2}$ emission was measured exciting the YAS: Ce^{3+}–Nd^{3+} bulk sample with a pulsed laser of 580 nm and detecting the temporal evolution decay at 850 nm. The decay values were fitted to a decreasing exponential, obtaining a mean lifetime of τ=157 μs, but the fit function did not match with the experimental results. Accordingly, the intensity decay values were fitted to Eq. (20) considering dipole-dipole interaction. The fit to the Inokuti-Hirayama model was in good agreement with the experimental values. This proves that non radiative energy transfer is taking place due to the high concentration of Nd^{3+} ions in the material. The values for the intrinsic lifetime and the energy transfer parameter were τ=260 μs and Q=0.81. Fig. 18 shows the experimental values for the temporal evolution of the intensity and the fitted curves to a decaying exponential and to the Inokuti-Hirayama model.

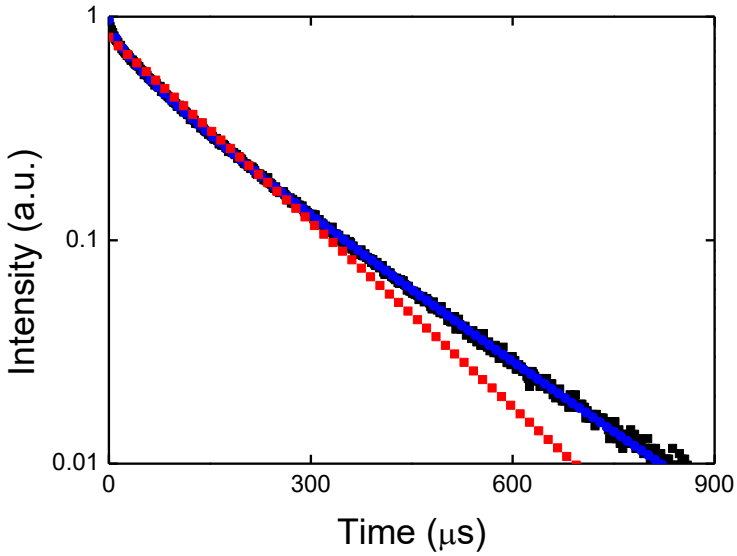

Figure 18. Temporal evolution decay of 850 nm emission of Nd^{3+} ions (black squares). Curve fitted to Inokuti model considering dipole-dipole interaction (blue squares) and to a decreasing exponential (red squares).

The temporal evolution of the upconversion emission was measured under 808 nm pulsed excitation. It shows an instantaneous increase and a decay with a fast and a slow components. The fast components is due to the direct excitation of the $^4G_{7/2}$ level with a lifetime of 0.54 μs and the slow component could be due to energy transfer processes from the $^4F_{3/2}$ level

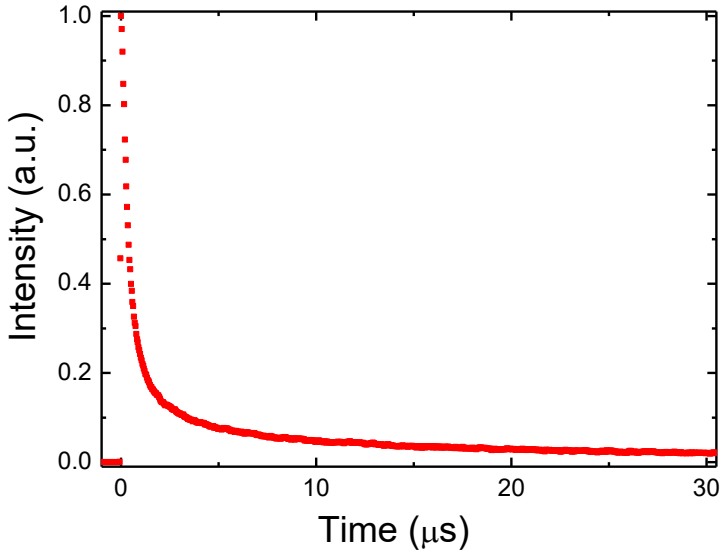

Figure 19. Temporal evolution of the upconversion emission of 530 nm of Nd^{3+} ions.

Conclusions

The transitions corresponding to the thermalized levels of neodymium ions were identified as $^4F_{5/2} \rightarrow ^4I_{9/2}$ (808 nm) and $^4F_{3/2} \rightarrow ^4I_{9/2}$ (890 nm). These levels were found suitable for the application of the Fluorescence Intensity Ratio technique due to the fact that their population distribution follows Boltzmann's law. In addition, the results obtained for the energy difference of the thermally coupled levels by means of the fit to a Boltzmann distribution (E_{32}=956cm^{-1}) and by absorption (E_{32}=1053cm^{-1}) are in good agreement. The absorption value could be improved by calculating the energy difference between the centroids of the emission bands instead of the maximum of the peaks.

The observation of whispering gallery modes was achieved placing the detection zone in the border of the sphere. The heating effects in the microsphere due to the laser source at 532 nm were studied. The variation of the ratio between the thermalized levels of neodymium was characterized and a maximum value for the sensitivity S_{FIR}=1.60 $\cdot 10^{-2}$ K^{-1} was found. A temperature resolution limit of $\Delta T_{min\ FIR}$ = 3 K was obtained for this technique. At the same time, the displacement of the whispering gallery modes was observed. It was concluded that the wavelength shift is not a constant parameter, obtaining greater values for the larger wavelength peaks. On the contrary, the sensitivity values were greater for the shorter wavelengths with a maximum value of S_{WGM}=15 $\cdot 10^{-6}$ K^{-1}. A temperature resolution limit $\Delta T_{min\ WGM}$ = 0.2 K was obtained for the WGM resonances in the 1300 nm band showing that the WGM displacement technique is an order of magnitude more accurate.

With the aim of studying the displacement of the whispering gallery modes in depth, an identification of the modes should have been done. For this purpose, transverse magnetic and electric modes should have been differentiated during the acquisition process. Microsphere with larger and shorter radius should be studied too.

Laser emission was observed under continuous pump in the emission band of $^4F_{3/2} \rightarrow ^4I_{11/2}$ (1064 nm) of Nd^{3+} ions with a threshold power of 100 mW. However, the conditions needed to obtain it have not been yet fully understood. More experiments must be performed with different excitation sources and with a mechanical chopper at different frequencies.

Upconversion emission was observed on microspheres under 808 nm laser excitation. The emission bands were also identified as $^4G_{7/2} \rightarrow ^4I_{9/2}$ (532 nm), $^4G_{7/2} \rightarrow ^4I_{11/2}$ (579 nm), $^4G_{7/2} \rightarrow ^4I_{13/2}$ (675 nm), $^4G_{7/2} \rightarrow ^4I_{9/2}$ (690 nm) and $^4G_{7/2} \rightarrow ^4I_{9/2}$ (750 nm). It was found that the first three bands were upconversion transitions while the other two were being populated by thermalization effects. It was concluded that two photons are required to obtain the upconversion emission. These spectra also presented the WGM resonances but the wavelength displacement with temperature could not be obtained because there was no thermal calibration for the levels involved. This thermal

calibration must be performed in order to compare the WGM displacement with temperature in all the spectrum.

From the fit of the temporal emission decay of the $^4F_{3/2}$ level to the Inokuti-Hirayama model, it was concluded that non radiative energy transfer processes were taking place due to the high concentrations of Nd^{3+} ions in the sample. More samples with different concentrations should be produced to determine which concentration of ions optimises the emission.

The measurement of the temporal evolution of the upconversion emission showed that ESA and ETU mechanisms are necessary to produce the upconversion process.

According to Ce^{3+} ions, further experiments must be performed to study the interaction with Nd^{3+} ions. Some emission spectra and intensity emission decay have been measured but not conclusions can be obtained.

References

[1] Ellen C. Jensen. “Use of Fluorescent Probes: Their Effect on Cell Biology and Limitations”. Anat. Rec. Volume 295, Issue 12, pages 2031–2036, December 2012

[2] Igor L. Medintz, H. Tetsuo Uyeda, Ellen R. Goldman & Hedi Mattoussi. “Quantum dot bioconjugates for imaging, labelling and sensing”. Nature Mat. 4, 435 - 446 (2005)

[3] J.-C.G. Bünzli. “Lanthanide Luminescence for Biomedical Analyses and Imaging.” Chem. Rev. 110, 2729–2755 (2010).

[4] Williamd, W. and Sudnick, D . “Lanthanide Ion Luminescence Probes of the Structure of Biological Macromolecules”. Acc. Chem. Res. 1981, 14, 384-392

[5] D. Jaque and F. Vetrone. “Luminescence nanothermometry.” Nanoscale. 4, 4301–4326 (2012).

[6]Tardieu F, Reymond M, Hamard P, Granier C, Muller B. “Spatial distributions of expansion rate, cell division rate and cell size in maize leaves: a synthesis of the effects of soil water status, evaporative demand and temperature”. J Exp Bot. 2000 Sep;51(350):1505-14

[7] V. K. Rai. “Temperature sensors and optical sensors,” Applied Physics. B 88(2), 297–303(2007).

[8] Pérez-Rodríguez C, Martín L L, León-Luis S F, Martín I R,Kumar K K and Jayasankar C K 2014 “Relevance of radiative transfer processes on Nd3+ doped phosphate glasses for temperature sensing by means of the fluorescence intensity ratio technique”. Sens-Actuators B Chem. 195 324–31

[9] Martín L. L, Haro-González P, Martín I R, Navarro-Urrios D,Alonso D, Pérez-Rodríguez C, Jaque D and Capuj N. E. 2011 “Whispering-gallery modes in glass microspheres: optimization of pumping in a modified confocal microscope”. Opt. Lett. 36 615–7

[10] S. A. Wade, Doctoral Dissertation (Victoria University, Melbourne, Australia, 1999).

[11] Wade S A, Collins S F and Baxter G W. “Fluorescence intensity ratio technique for optical fiber point temperature sensing”. J. Appl. Phys. 94 474

[12]S.F. Coums, G.W. Baxter, S.A. Wade, T. Sun, K.T.V. (jrattan, Z.Y. Zhang and A.W, Pahner, "Comparison of fluorescence-based temperature sensor schemes:theoretical analysis and experimental validation", J. Appl. Phys., 84, pp. 4649-4654,1998.

[13] Yutian, W. and Likun, G. “Rare Earth Doped Optical Fibers for Temperature Sensing Utilizing Ratio-Based Technology”. J. RARE EARTHS Vol. 24, Spec. Issue, Dec . 2006, p .171

[14]Vahala, K. J. “Optical microcavities” Nature 424 839–46 2003

[15] A. B. Matsko, A. A. Savchenkov, D. Strekalov, V. S. Ilchenko, and L. Maleki, “Review of Applications of Whispering-Gallery Mode Resonators in Photonics and Nonlinear Optics,” IPN Progress Report 42-162 (2005), pp. 1–51.

[16] L.Yang and K. J. Vahala, "Gain functionalization of silica microresonators," Opt. Lett. 28, 592-594 (2003)

[17]W. Koechner and M. Bass. “Solid-State Lasers: A Graduate Text”. Springer. 2003

[18] X. Wei-Dong, Z. Bin-Yu, L. Xiao-Juan, C. Zhao-Ping, X. Cui-Ping, LUO Le, Z. Zhi-Min, Z. Jing-Feng, Z. Jia-Song. “Packaging Technologies and Luminescence Properties of Ce:YAG Single Crystal for White Light-emitting Diode”. JIM, 2014, 29(6): 614-620

[19] W. Zhou, J. Yang, J. Wang, Y. Li, Xi. Kuang, J. Tang, and H. Liang, "Study on the effects of 5d energy locations of Ce^{3+} ions on NIR quantum cutting process in Y_2SiO_5: Ce^{3+}, Yb^{3+}," Opt. Express20, A510-A518 (2012)

[20] J. Méndez-Ramos, M. Abril, I. R. Martín, U. R. Rodríguez-Mendoza, V. Lavín, and V. D. Rodríguez. “Ultraviolet and visible upconversion luminescence in Nd^{3+} -doped oxyfluoride glasses and glass ceramics obtained by different preparation methods” J. Appl. Phys. 99, 113510 (2006)

[21] M. Inokuti and F. Hirayama. “Influence of Energy Transfer by the Exchange Mechanism on Donor Luminescence.” J. Chem. Phys. 43, 1978 (1965).

[22] G. Adamovsky and M. V. Otugen, “Morphology-dependent resonances and their applications to sensing in aerospace environments,” J. Aerosp. Comp. Inf. Commun. 5(10), 409–424 (2009).

[23] Kippenberg, T.J.A., “Nonlinear Optics in Ultra-High-Q Wispering Gallery Optical Microcavities,” Doctoral Dissertation, California Institute of Technology

[24] T. Ioppolo, N. Das, and M. Volkan Ötügen.” Whispering gallery modes of microspheres in the presence of a changing surrounding medium: A new ray-tracing analysis and sensor experiment” J. Appl. Phys. 107. 103105

[25] Sanditov D S and Sydykov B S “Modulus of elasticity and thermal expansion coefficient of glassy solids” Phys. Solid State 56 1006–8

[26] Q. Ma, T. Rossmann, and Z. Guo, “Temperature sensitivity of silica micro-resonators,” J. Phys. D Appl. Phys.41(24), 245111 (2008)

[27] G. R. Elliott, D. W. Hewak, G. S. Murugan, and J. S. Wilkinson, “Chalcogenide glass microspheres; their production, characterization and potential,” Opt. Express 15(26), 17542–17553 (2007)

[28] M. White Ian , M. Hanumegowda Niranjan, Oveys Hesam, and Fan Xudong 2005. “Whispering gallery modes in a glass microsphere as a function of temperature”. Opt. Express 13 10754–10759

[29] G.N. Atroshchenko and V.N. Sigaev. “Glassy microspheres and their applications in nuclear medicine (review)”. Glass and Ceramics. Vol. 72 397 – 404 (2016)

[30] F. Vollmer and S. Arnold, “Whispering-gallery-mode biosensing: label-free detection down to single molecules,”Nat. Methods **5**(7), 591–596 (2008).

[31] Arnold, S., Ramjit, R., Keng, D., Kolchenko, V. & Teraoka, I. Microparticle photophysics illuminates viral biosensing. *Faraday Discuss.* **137**, 65–83 (2008).

[32] L. L. Martín, D. Navarro-Urrios, F. Ferrarese-Lupi, C. Pérez-Rodríguez, I R Martín, J. Montserrat, C Dominguez, B. Garrido and N. Capuj. "Laser emission in Nd3+ doped barium–titanium–silicate microspheres under continuous and chopped wave pumping in a non-coupled pumping scheme." Laser Phys. 23 (2013) 075801